

## Low- and high-thermogenic brown adipocyte subpopulations coexist in murine adipose tissue

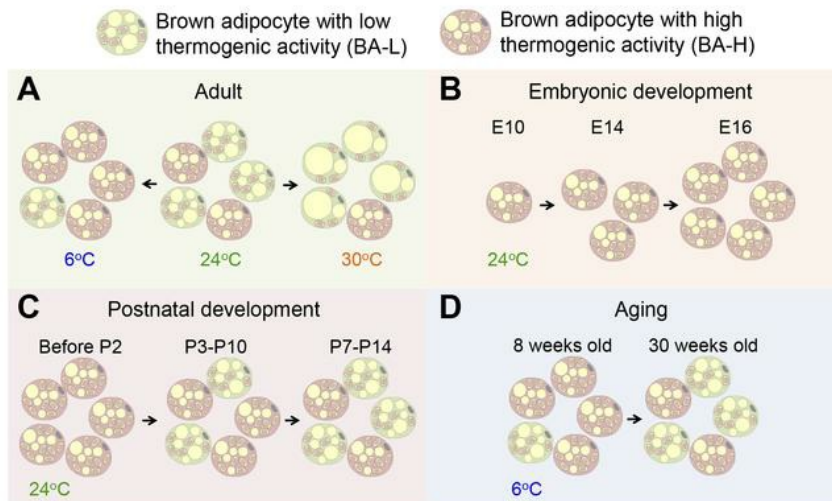
Anying Song, ... , Philipp E. Scherer, Qiong A. Wang

*J Clin Invest.* 2019. <https://doi.org/10.1172/JCI129167>.

Research In-Press Preview Metabolism

### Graphical abstract

#### Graphical Abstract



Find the latest version:

<https://jci.me/129167/pdf>



# Low- and high-thermogenic brown adipocyte subpopulations coexist in murine adipose tissue

Anying Song<sup>1</sup>, Wenting Dai<sup>1</sup>, Min Jee Jang<sup>2</sup>, Leonard Medrano<sup>3</sup>, Zhuo Li<sup>4</sup>, Hu Zhao<sup>5</sup>, Mengle  
Shao<sup>6</sup>, Jiayi Tan<sup>1</sup>, Aimin Li<sup>7</sup>, Tinglu Ning<sup>1</sup>, Marcia M. Miller<sup>4</sup>, Brian Armstrong<sup>8</sup>, Janice M. Huss<sup>1</sup>,  
5 Yi Zhu<sup>9</sup>, Yong Liu<sup>10</sup>, Viviana Gradinaru<sup>2</sup>, Xiwei Wu<sup>11</sup>, Lei Jiang<sup>1,12</sup>, Philipp E. Scherer<sup>6</sup>, Qiong  
A. Wang<sup>1,12\*</sup>

<sup>1</sup>Department of Molecular & Cellular Endocrinology, Diabetes and Metabolism Research Institute,  
<sup>3</sup>Division of Developmental and Translational Diabetes and Endocrinology Research, <sup>4</sup>The  
10 Electron Microscopy and Atomic Force Microscopy Core, <sup>7</sup>Pathology Core of Shared resources,  
<sup>8</sup>The Light Microscopy Core, <sup>11</sup>The Integrative Genomics Core, <sup>12</sup>Comprehensive Cancer Center,  
Beckman Research Institute, City of Hope Medical Center, Duarte, California 91010, USA.

<sup>2</sup>Division of Biology and Biological Engineering, California Institute of Technology, Pasadena,  
California 91125, USA.

15 <sup>5</sup>Department of Restorative Sciences, School of Dentistry, Texas A&M University, Dallas, Texas,  
75246, USA.

<sup>9</sup>Children's Nutrition Research Center, Department of Pediatrics, Baylor College of Medicine,  
Houston, Texas, 77030, USA

20 <sup>10</sup>Hubei Key Laboratory of Cell Homeostasis, College of Life Sciences, Institute for Advanced  
Studies, Wuhan University, Wuhan 430072, China.

<sup>6</sup>Touchstone Diabetes Center, University of Texas Southwestern Medical Center, Dallas, Texas,  
75390, USA.

25 \*Correspondence should be addressed to:

Qiong (Annabel) Wang, Department of Molecular & Cellular Endocrinology, City of Hope.  
1500 East Duarte Road, Duarte, CA 91010  
E-mail: [qwang@coh.org](mailto:qwang@coh.org); Phone: 626-218-6419

30 Conflict of interest: The authors have declared that no conflict of interest exists.

## Abstract

Brown adipose tissue (BAT), as the main site of adaptive thermogenesis, exerts beneficial metabolic effects on obesity and insulin resistance. BAT has been previously assumed to contain a homogeneous population of brown adipocytes. Utilizing multiple mouse models capable of genetically labeling different cellular populations, as well as single-cell RNA sequencing, and 3D tissue profiling, we discovered a new brown adipocyte subpopulation with low thermogenic activity co-existing with the classical high thermogenic brown adipocytes within the BAT. These low thermogenic brown adipocytes had significantly lower *Ucp1* and *Adipoq* expression, larger lipid droplets, and lower mitochondrial content. Functional analyses showed that the low thermogenic brown adipocytes have significant lower basal mitochondrial respiration, and they are specialized in fatty acid uptake. Upon changes in environmental temperature, the two brown adipocyte subpopulations underwent dynamic inter-conversions. Cold exposure converted low thermogenic brown adipocytes into high thermogenic cells, and a thermoneutral environment had the opposite effect. This recruitment of high thermogenic brown adipocytes by cold stimulation is not affected by high fat diet feeding, but significantly declined with age. Our results revealed a high degree of functional heterogeneity of brown adipocytes.

**185 words**

## Introduction

Brown adipose tissue (BAT) is a thermogenic organ that is thought to play an important role in human energy homeostasis (1-3). Upon activation, brown adipocytes within the BAT can function as an effective energy sink, burning and disposing excess lipids and glucose (4-6). In recent years, progress has been made in rodents and humans in understanding the function and physiological impact of BAT. It is now well accepted that recruiting and activating BAT can correct dyslipidemia and prevent obesity-related metabolic disorders (7-10). Although functional heterogeneity has recently been reported in white and beige adipocytes within an individual fat depot (11-14), BAT is still viewed to have a highly homogeneous population of brown adipocytes. Interestingly, some previous studies have indicated that thermogenesis is not uniformly activated in all brown adipocytes. For instance, brown adipocytes have been shown to have a heterogeneous expression of Uncoupling Protein 1 (UCP1) (15, 16). Moreover, in vitro cultured brown adipocytes showed heterogeneous mitochondrial membrane potential (17, 18). However, the thermogenic and metabolic heterogeneity of brown adipocytes within the same BAT in vivo remains largely uncharacterized.

## Results

To better understand brown adipocyte dynamics in vivo, we used the AdipoChaser-LacZ mouse model we previously developed to label brown adipocytes. This model is a doxycycline (dox)-based, tet-responsive labeling system for the inducible, permanent labeling of Adiponectin (*Adipoq*) expressing cells as LacZ<sup>+</sup> cells (Supplemental Figure 1A) (19, 20). To our surprise, at room temperature (24°C), despite the uniform labeling of white adipocytes (19, 20), only 38% of total brown adipocytes in the BAT were labeled as LacZ<sup>+</sup> (blue) cells, and these cells distribute in

75 a patchy pattern (Figure 1, A and B). The percentage of LacZ<sup>+</sup> brown adipocytes is significantly higher (76%) when mice were housed in a cold environment (6°C), and significantly lower (6%) when mice were housed in a thermoneutral environment (30°C) (Figure 1, A and B). However, *Adipoq* mRNA in the whole BAT was slightly increased when mice were at 6°C, and was not altered when mice were in 30°C (Supplemental Figure 1B). When we treated AdipoChaser-LacZ  
80 mice with β<sub>3</sub>-adrenergic receptor agonist to stimulate thermogenesis (Figure 1C), we observed a similar percentage of LacZ<sup>+</sup> brown adipocytes as upon cold exposure (67%) (Figure 1, D and E).

Is the increase of LacZ<sup>+</sup> brown adipocytes during cold exposure due to *de novo* adipogenesis? And likewise, is the decrease of LacZ<sup>+</sup> brown adipocytes during thermoneutral exposure due to  
85 cell death? When we pre-labeled mice at 24 °C and pulse-chased at 6°C or 30°C, the percentages of LacZ<sup>+</sup> brown adipocytes (40%) remained the same as when they were at 24°C (Figure 1, F and G). When we pre-labeled mice at 30°C and pulse-chased at 6°C, the percentages of LacZ<sup>+</sup> brown adipocytes (5%) remained the same as when they were at 30°C (Figure 1H). Likewise, when we pre-labeled mice at 6°C and pulse-chased at 30°C, the percentages of LacZ<sup>+</sup> brown adipocytes  
90 (73%) remained the same as when they were at 6°C (Figure 1I). Meanwhile, body weight, BAT weight, and brown adipocyte cell size were not altered when mice were in a cold environment (Supplemental Figure 1, C–E). Moreover, we have not observed significant apoptosis of brown adipocyte by active Caspase 3 staining (Supplemental Figure 2, A–D). Therefore, there are dynamic inter-conversions between these two brown adipocyte subpopulations upon temperature  
95 change, and we have no evidence of significant adipogenesis or cell death.

We subsequently looked into the subcellular structure of these two brown adipocyte

subpopulations through electron microscopy imaging. X-gal, when cleaved by  $\beta$ -galactosidase, produces 5,5'-dibromo-4,4'-dichloro-indigo-2, an intense blue product which is insoluble. Under the electron microscope, this blue product can be observed as crystals (21, 22), and the LacZ+ brown adipocytes can be distinguished by this feature. Compared to the LacZ+ brown adipocytes (adiponectin high-expressing), the LacZ- brown adipocytes had significantly lower mitochondrial number/content and much larger lipid droplets (Figure 2, A–D). We then switched to an AdipoChaser-mT/mG system we reported recently (20, 23) (Supplemental Figure 3A), and confirmed that *Adipoq* is selectively expressed in a subpopulation of brown adipocytes in a patchy pattern (Supplemental Figure 3, B and C). In the isolated primary brown adipocytes, the GFP- (*Adipoq* low-expressing) brown adipocytes had significantly higher mitochondrial membrane potential (Supplemental Figure 3, D–F), indicating that these cells have lower mitochondrial membrane depolarization and uncoupling rate (24). We also generated the AdipoChaser-YFP mice (Supplemental Figure 3G), as YFP is relative easier for immunofluorescence staining. When we labeled mice in 6°C, the *Adipoq* high-expressing (YFP+) brown adipocytes largely overlapped with UCP1 high expressing cells (Figure 2E). Thus, *Adipoq* expression positively correlates with UCP1 protein expression. Overall, these results suggest that the *Adipoq* low-expressing brown adipocytes are morphologically and molecularly different from the *Adipoq* high-expressing brown adipocytes. When we pre-labeled mice at 24°C and pulse-chased at 6°C, there were significantly more UCP1+ cells than YFP+ cells, and most of the pre-labeled YFP+ brown adipocytes co-labeled as UCP+ cells (Figure 2F). This result confirms that the YFP- brown adipocytes labeled at 24°C could convert into UCP1 high expressing cells at 6 °C.

120 We next set out to verify the brown adipocyte heterogeneity through single-cell RNA-sequencing  
(scRNA-seq) of primary brown adipocytes isolated from the BAT of adult mice housed at 24°C.  
Two major brown adipocyte subpopulations were clustered: brown adipocytes with high  
thermogenic activity (BA-H, 2,352 cells, including three sub-clusters, BA-H1, BA-H2, and BA-  
H3) and brown adipocytes with low thermogenic activity (BA-L, 1,250 cells) (Figure 3A). These  
125 two populations differed by the expression level of *Ucp1*, as well as *Adipoq* (Figure 3, B and C).  
Two other clusters of cells were identified as white adipocytes (WA, 197 cells) and non-adipocytes  
(NA, 34 cells) (Figure 3A). This white adipocyte cluster served as a nice internal control in the  
subsequent analysis. In the BA-L subpopulation, expressions of genes related to thermogenesis,  
such as *Cidea*, *Elovl6*, and oxidative phosphorylation (OXPHOS) complexes were extremely low,  
130 close or lower than the white adipocytes in the WA cluster (Figure 3D, Supplemental Figure 4 and  
Supplemental Figure 5, A–E). Similarly, the BA-L subpopulation had very low expression levels  
of genes related to lipolysis, glycolysis, fatty acid oxidation, and the TCA cycle (Figure 3E and  
Supplemental Figure 6, A–C). Moreover, two newly identified pathways that have been described  
and may be essential for the positive regulation of thermogenesis, ROS (25) and succinate  
135 metabolism (26), were also only enriched in the BA-H subpopulation (Supplemental Figure 6, D  
and E). Therefore, brown adipocytes within the BA-L subpopulation belong to a novel and unique  
type of brown adipocyte with low thermogenic activity.

Notably, the BA-L subpopulation had significant high expression levels of genes related to fatty  
140 acid uptake (Figure 2F and Supplemental Figure 7A). This subpopulation was also enriched for  
genes that are essential for cell-to-cell trafficking (27) (Supplemental Figure 7B), as well as UCP1-  
independent thermogenesis through the futile cycle of creatine metabolism (28) and tight junction

(Supplemental Figure 7, C and D). Thus, brown adipocytes within the BA-L subpopulation hold a unique metabolic status, and the function of these cells is potentially fundamentally different from the cells within the BA-H subpopulation.

What regulates the functional heterogeneity between the two brown adipocyte subpopulations? Interestingly, PPAR $\gamma$  (29) and C/EBP $\alpha$  (30), the two master transcription factors that regulate adipocyte function (31, 32), have distinct expression patterns in these two subpopulations. Surprisingly, *Pparg* was relatively enriched in the BA-L subpopulation (Supplemental Figure 7E), consistent with the expression patterns of its downstream targets *Cd36* and *Fabp4* (Figure 2F). In contrast, *Cebpa* was enriched in the BA-H subpopulation (Supplemental Figure 7E). These data indicate that these two factors may act as upstream regulators responsible for the distinct transcriptional profiles of the two brown adipocyte subpopulations. As expected, the expression of white adipocyte marker resistin (*Retn*) (Supplemental Figure 7F) was only detected in the WA cluster. Among the three BA-H sub-clusters, thermogenic genes had the highest expression levels in BA-H3 (Supplemental Figure 4). The sub-clusters BA-H1 and BA-H2 were enriched for genes that related to mitochondrial biogenesis and insulin responsiveness (33-35) (Supplemental Figure 7H).

We next performed immunofluorescence co-staining to confirm the protein levels of these genes identified through scRNA-seq. In the AdipoChaser-YFP mice (Figure 4A), YFP<sup>+</sup> cells (*Adipoq* high expressing brown adipocytes) primarily overlapped with *Elovl6* (Figure 4B), as well as SDHA and COX IV (Figure 4, C and D); while large numbers of YFP<sup>+</sup> brown adipocytes did not

165 overlap with FABP4 (Figure 4E), as well as PPAR $\gamma$  (Figure 4F). Thus, the protein levels of these important genes match with the expression pattern demonstrated by the scRNA-seq results.

To test whether the two brown adipocyte subpopulations have different mitochondrial respiratory capacity, we separately collected the two freshly isolated brown adipocyte subpopulations from  
170 BAT through mild centrifugation. With the *Ucp1*-GFP mice, a tet-responsive labeling system under the control of the *Ucp1* promoter (Figure 5A), isolation and separation were verified based on the GFP signal intensity (Figure 5B). We first measured mitochondrial function through a Mito Stress Test Kit (Figure 5C). The BA-H, BA-L, white adipocyte, and primary BAT stromal vascular fraction (SVF) showed distinct levels of oxygen consumption as judged by the oxygen  
175 consumption rate (OCR). As the ATP synthesis rate is relatively low in brown adipocytes due to uncoupled respiration, it is not surprising that oligomycin (ATP synthase inhibitor) did not significantly alter OCR in brown adipocytes; while oligomycin decreased OCR by 59% in SVF, and by 20% in white adipocyte (Figure 5C). The basal respiration in the BA-H population was around two-fold higher compared to the BA-L population. Both brown adipocyte subpopulations  
180 had significantly higher basal respiration compared to white adipocyte and the SVF (Figure 5D). Interestingly, the BA-H population had a maximal respiration rate very close to the BA-L population, indicating these brown adipocytes have high mitochondrial potential and are readily recruitable (Figure 5E). The BA-H population isolated through mild centrifugation contains a low percentage of SVF. To obtain a purer BA-H population, we isolated the BA-H population from  
185 AdipoChaser-mT/mG mice through a magnetic bead-based method taking advantage of the membrane-bound GFP. The OCR levels of both BA-L and BA-H subpopulations obtained through this alternative method were much lower compared to the cells obtained through mild

centrifugation, which may due to the much longer processing time involved for the isolation (Figure 5F). However, the difference in basal OCR is consistent between the two methods (Figure 5C and Figure 5F). Moreover, both BA-L and BA-H populations showed responses to norepinephrine, but the BA-H population had a more robust increase in the OCR (Figure 5F). We also measured the fatty acid uptake rate in the two brown adipocyte subpopulations, and consistent with the high *Fabp4* mRNA and protein level (Figure 3F and Figure 4D), the BA-L population displayed significantly higher rates of fatty acid uptake (Figure 5G). This result is consistent with a recent report, which demonstrated that the uptake of nutrients by adjacent murine brown adipocytes is variable (36). Overall, these results demonstrate that the two brown adipocyte subpopulations have fundamentally distinct function and metabolic profiles.

We performed 3D profiling of BAT from the *Ucp1*-GFP mice housed at 24 °C. UCP1+ (GFP+) brown adipocytes distributed in a patchy pattern (Figure 5H and Supplemental Video 1), confirming the scRNA-seq result that *Ucp1* is also distinctly expressed in different subpopulations of brown adipocytes. The thermogenesis of brown adipocytes is governed by sympathetic innervation (37). The 3D architecture showed that compared to the less innervated white adipose tissues (38, 39), almost every brown adipocyte is heavily innervated with sympathetic neurons (Figure 5H and Supplemental Video 1). Thus, the diversity in thermogenic activity observed in these two brown adipocyte subpopulations is not determined by sympathetic innervation. Notably, the expression level of  $\beta$ 3-adrenergic receptor *Adrb3* was enriched in the BA-H subpopulation (Supplemental Figure 7G). Therefore, the diverse thermogenic activity may be determined by the difference in the responsiveness of brown adipocyte to  $\beta$ 3-adrenergic signals.

Does BAT emerge developmentally as two distinct subpopulations? We looked into the *Adipoq* expression in brown adipocytes during development, by exposing AdipoChaser-LacZ mice to dox diet at various embryonic and postnatal stages (Figure 6A). When we exposed mice to dox diet during E3–10, very few (less than 1%) of brown adipocytes were labeled as LacZ<sup>+</sup> cells upon examining the tissue at 4 weeks of age (Figure 6B). When mice were exposed to dox diet during E7–E14, brown adipocytes showed a heterogeneous pattern of LacZ<sup>+</sup> cells, with some regions carrying more than 92%, and other regions displaying less than 10% LacZ<sup>+</sup> signal when examined at 4 weeks of age (Figure 6C). When mice were exposed to dox diet during E9–E16, brown adipocytes showed uniform positive labeling of LacZ<sup>+</sup> cells when examined at 4 weeks of age (Figure 6D). These observations indicate that brown adipocytes differentiation is initiated as early as E10, and all brown adipocytes have initiated differentiation and started to express *Adipoq* by E16. Thus, adiponectin can be used as a terminal differentiation marker for both brown adipocytes as well as for white adipocytes (19). At the age of 27 weeks, for the mice that were exposed to dox diet during E18–P4, the brown adipocytes continued to display a uniformly positive LacZ labeling (Figure 6E), indicating that the turnover rate for brown adipocytes is extremely low in the adult stage at room temperature. Thus, the *Adipoq* low-expressing brown adipocytes are not newly generated postnatally.

We subsequently narrowed down the time frame during which the BAT develops heterogeneity through the inter-conversion (Figure 6F). When AdipoChaser-LacZ mice were exposed to dox diet during E7–P2, their brown adipocytes showed a uniform LacZ<sup>+</sup> labeling when examined at 8 weeks of age (adult stage) (Figure 6G). When mice were exposed to dox diet during P3–P10 or P7–P14, 56% or 42% of their brown adipocytes were labeled as LacZ<sup>+</sup> cells, which is close to the

percentage at the adult stage (38% in Figure 1B). These experiments indicate that the BAT  
235 transcriptional program becomes heterogeneous shortly after birth, and the ratio of *Adipoq* high-  
expressing and low-expressing brown adipocytes becomes stable around P7.

It has been suggested that decreased BAT thermogenesis is associated with the accumulation of  
body fat, as well as age (40-42). Therefore, we checked if high fat diet (HFD) induced obesity  
240 reduces the inter-conversion of *Adipoq* low expressers to high expressers during cold exposure  
(Supplemental Figure 8, A and B). When AdipoChaser-LacZ mice were housed at 6°C, the  
percentages of LacZ<sup>+</sup> brown adipocytes from HFD fed mice (47%) were comparable to brown  
adipocytes from chow-fed mice (45%) (Supplemental Figure 8, C and D). At 24°C, HFD fed mice  
even had higher percentages of LacZ<sup>+</sup> brown adipocytes (23% Vs. 12%). Thus, HFD feeding does  
245 not impair the recruitment of *Adipoq* high-expressing brown adipocytes during cold exposure.  
However, even in the chow-fed group, these 21-week-old mice had a significantly lower  
percentage of LacZ<sup>+</sup> brown adipocytes at both 6°C and 24°C compared to 8-week-old mice (Figure  
1, A and B), indicating that there is a decline in the number of *Adipoq* high expressers with age.  
When older mice were housed at 6°C (Figure 7A), the percentage of LacZ<sup>+</sup> brown adipocytes  
250 further dropped to below 40% (30-week-old) and 20% (60-week-old) (Figure 7, B and C). These  
results indicate that the ability of BAT to recruit *Adipoq* high-expressing brown adipocytes during  
cold exposure is significantly reduced with age.

## Discussion

255 We report the discovery of a low-thermogenic brown adipocyte subpopulation with unique  
molecular and metabolic features, co-existing with the classic brown adipocytes in vivo. The

results presented here offer critical insights towards our understanding of how brown adipose tissue thermogenesis is regulated at the cellular level. The discovery of the new low thermogenic subpopulation is of great interest since this population of cells does not have typical brown adipocyte morphology and display a unique metabolic profile. However, the exact function of this subpopulation is largely unknown. These brown adipocytes have relative large lipid droplets and low mitochondrial content and extremely low respiration rate, compared to the high thermogenic subpopulation. Are these brown adipocytes in a “resting” status and are readily recruitable to convert into high thermogenic cells? Or do they have critical metabolic functions other than thermogenesis? As the low thermogenic brown adipocytes have a much higher rate of fatty acid intake, these cells may have an indispensable role for the functional integrity of the thermogenic activity of the whole BAT. The high thermogenic subpopulation represents the extensively studied classic brown adipocyte subtype, which has the potential ability to further increase *Ucp1* expression and thermogenesis upon cold stimulation. It is worth to note that most of the human studies detect BAT based on glucose uptake, as BAT exhibits high uptake of fluorine-18 fludeoxyglucose on positron emission tomography (PET). This detection method may miss the lower thermogenic brown adipocytes, which have high fatty acid uptake rate.

Adiponectin is considered a white adipocyte marker since it is more abundantly expressed in the white adipocyte. However, it is not surprising to observe a higher *Adipoq* expression in the high thermogenic brown adipocytes, as adiponectin positively regulates mitochondrial biogenesis and activity (43-45). Recent 3-D adipose tissue imaging reveals that cold-induced generation of beige adipocytes in the subcutaneous adipose tissue depends on the density of sympathetic innervation (38, 39). Here, we show that sympathetic innervation in BAT is much denser than that in white

280 adipose tissue. Thus, the thermogenic heterogeneity of brown adipocytes is not correlated to sympathetic innervation. However, it is still possible that norepinephrine is differentially secreted by each sympathetic neuron. Notably, the expression level of  $\beta$ 3-adrenergic receptor *Adrb3* was enriched in the BA-H subpopulation. Therefore, the diverse thermogenic activity may be determined by the difference in the responsiveness of brown adipocyte to  $\beta$ 3-adrenergic signals.

285 Developmentally, as newborn pups require much higher thermogenic activity, it is not surprising that all brown adipocytes are born as *Adipoq* high expressers and potentially have high thermogenic activity. Interestingly, a subpopulation of brown adipocytes gradually converts into *Adipoq* low expressers after birth. The establishment of heterogeneity postnatally is likely due to  
290 the heterogeneous lineages of brown adipocyte precursors during development. However, it is also possible that the two brown adipocyte subpopulations are not born to be different, and they may undergo a “switching mechanism” even at room temperature, taking dynamic turns to function as high thermogenic cells. As the interscapular BAT is the first adipose depot to develop in the mouse, BAT may serve as the primary site for adiponectin expression and secretion in these very early  
295 stages of life. When white adipose depots development initiates later in life, these tissues then take over as the primary sites for adiponectin production. When mice in the adult stage are exposed to cold, other than a conversion of BA-L into BA-H population, BAT may also undergo *de novo* adipogenesis, especially when mice are exposed to the cold for a long period of time (46, 47). Importantly, the conversion of low thermogenic brown adipocytes into high thermogenic  
300 adipocytes upon cold exposure is impaired with old age, but not by high fat diet feeding. This may offer a new explanation for the age-associated decline in brown adipose tissue thermogenic activity.

305 Future studies will need to address the metabolic functions and lineages of the low thermogenic brown adipocyte subpopulation, as well as the molecular mechanisms that regulate the inter-conversion between the two subpopulations. More importantly, it will be interesting to determine why the number of thermogenic high brown adipocytes declines with age. Unmasking the complex physiology of BAT thermogenesis is essential to improve our ability to identify effective therapeutic approaches for metabolic disorders. Future strategies that promote the low thermogenic brown adipocytes to convert into a population of high thermogenic cells may greatly enhance brown adipose tissue thermogenesis, which may have potential for the treatment of obesity and diabetes.

## Methods

315 Detailed methods are in the Supplemental Material.

The scRNA-seq data have been deposited in NCBI GEO with the access number GSE125269.

*Statistics.* The results are shown as means  $\pm$  sd. Differences were analyzed by various methods as indicated in figure legends. All measurements were taken from individual samples.

320

*Study approval.* The Institutional Animal Care and Use Committees of City of Hope, Duarte, have approved all animal experiments.

### **Author contributions**

325 Q.A.W., P.E.S., and A.S. designed the experiments. Q.A.W., P.E.S., and L.J. wrote the manuscript.  
A.S., T.N., and Q.A.W. handled all the mouse experiments and performed  $\beta$ -gal staining. A.S.  
performed the mitochondrial membrane potential test and immunofluorescence staining. A.S.  
prepared primary brown adipocytes and X.W. conducted and analyzed scRNA-seq experiments.  
A.S., Q.A.W., and W.D. performed the seahorse and fatty acid intake experiment. A.S., M.J., H.Z.,  
330 and B.A. performed BAT tissue clearing and three-dimensional imaging. A.S., Z.L., and M.M.  
performed the transmission electron microscopy. M.S., Y.L., Y.Z., and V.G. contributed to  
experimental design and discussion. All authors approved the final manuscript.

### **Acknowledgments**

335 The authors are grateful to Jiandie Lin, Li Ye, and members of the Diabetes and Metabolism  
Research Institute for discussions and comments. The authors thank the City of Hope Animal  
Resource Center, Integrative Genomics Core, Electron Microscopy and Atomic Force Microscopy  
Core, Light Microscopy Core, Pathology (Solid Tumor) Core (supported by NIH P30CA033572),  
Analytical Cytometry Core, and City of Hope Comprehensive Cancer Center for guidance and  
340 assistance for experiments. This study was supported by US National Institutes of Health grants  
K01DK107788, R03HD095414, and R56AG063854 to Q.A.W.; R01DK55758, R01DK099110,  
P01DK088761 and P01AG051459 to P.E.S.. Q.A.W. was also supported by City of Hope Caltech-  
COH Initiative Award, and American Diabetes Association Junior Faculty Development Award  
1-19-JDF-023. P.E.S. was also supported by an unrestricted research grant from the Novo Nordisk  
345 Foundation.

## References

1. Orava J, Nuutila P, Lidell ME, Oikonen V, Nojonen T, Viljanen T, et al. Different metabolic responses of human brown adipose tissue to activation by cold and insulin. *Cell metabolism*. 2011;14(2):272-9. 350
2. Ouellet V, Labbé SM, Blondin DP, Phoenix S, Guérin B, Haman F, et al. Brown adipose tissue oxidative metabolism contributes to energy expenditure during acute cold exposure in humans. *The Journal of clinical investigation*. 2012;122(2):545-52.
3. Chondronikola M, Volpi E, Børsheim E, Porter C, Annamalai P, Enerbäck S, et al. Brown adipose tissue improves whole body glucose homeostasis and insulin sensitivity in humans. 355 *Diabetes*. 2014:DB\_140746.
4. Bartelt A, Bruns OT, Reimer R, Hohenberg H, Ittrich H, Peldschus K, et al. Brown adipose tissue activity controls triglyceride clearance. *Nat Med*. 2011;17(2):200-5.
5. Stanford KI, Middelbeek RJ, Townsend KL, An D, Nygaard EB, Hitchcox KM, et al. 360 Brown adipose tissue regulates glucose homeostasis and insulin sensitivity. *The Journal of clinical investigation*. 2012;123(1).
6. Chouchani ET, Kazak L, and Spiegelman BM. New Advances in Adaptive Thermogenesis: UCP1 and Beyond. *Cell Metabolism*. 2018.
7. Lowell BB, Vedrana S, Hamann A, Lawitts JA, Himms-Hagen J, Boyer BB, et al. 365 Development of obesity in transgenic mice after genetic ablation of brown adipose tissue. *Nature*. 1993;366(6457):740.
8. Kopecky J, Clarke G, Enerback S, Spiegelman B, and Kozak LP. Expression of the mitochondrial uncoupling protein gene from the aP2 gene promoter prevents genetic obesity. *J Clin Invest*. 1995;96(6):2914-23.

- 370 9. Crane JD, Palanivel R, Mottillo EP, Bujak AL, Wang H, Ford RJ, et al. Inhibiting peripheral serotonin synthesis reduces obesity and metabolic dysfunction by promoting brown adipose tissue thermogenesis. *Nature medicine*. 2014.
10. Gnad T, Scheibler S, von Kugelgen I, Scheele C, Kilic A, Glode A, et al. Adenosine activates brown adipose tissue and recruits beige adipocytes via A2A receptors. *Nature*. 2014;516(7531):395-9.
- 375 11. Bertholet AM, Kazak L, Chouchani ET, Bogaczynska MG, Paranjpe I, Wainwright GL, et al. Mitochondrial Patch Clamp of Beige Adipocytes Reveals UCP1-Positive and UCP1-Negative Cells Both Exhibiting Futile Creatine Cycling. *Cell Metab*. 2017;25(4):811-22.e4.
- 380 12. Lee KY, Sharma R, Gase G, Ussar S, Li Y, Welch L, et al. Tbx15 Defines a Glycolytic Subpopulation and White Adipocyte Heterogeneity. *Diabetes*. 2017;66(11):2822-9.
13. Lee KY, Luong Q, Sharma R, Dreyfuss JM, Ussar S, and Kahn CR. Developmental and functional heterogeneity of white adipocytes within a single fat depot. *EMBO J*. 2018.
14. Chen Y, Ikeda K, Yoneshiro T, Scaramozza A, Tajima K, Wang Q, et al. Thermal stress induces glycolytic beige fat formation via a myogenic state. *Nature*. 2019;565(7738):180-5.
- 385 15. Cinti S, Cancellato R, Zingaretti MC, Ceresi E, De Matteis R, Giordano A, et al. CL316,243 and cold stress induce heterogeneous expression of UCP1 mRNA and protein in rodent brown adipocytes. *J Histochem Cytochem*. 2002;50(1):21-31.
- 390 16. Spaethling JM, Sanchez-Alavez M, Lee J, Xia FC, Dueck H, Wang W, et al. Single-cell transcriptomics and functional target validation of brown adipocytes show their complex

roles in metabolic homeostasis. *FASEB journal : official publication of the Federation of American Societies for Experimental Biology*. 2016;30(1):81-92.

- 395 17. Wikstrom JD, Mahdavian K, Liesa M, Sereda SB, Si Y, Las G, et al. Hormone-induced mitochondrial fission is utilized by brown adipocytes as an amplification pathway for energy expenditure. *EMBO J*. 2014;33(5):418-36.
18. Xie T-R, Liu C-F, and Kang J-S. Sympathetic transmitters control thermogenic efficacy of brown adipocytes by modulating mitochondrial complex V. *Signal Transduction And Targeted Therapy*. 2017;2:17060.
- 400 19. Wang QA, Tao C, Gupta RK, and Scherer PE. Tracking adipogenesis during white adipose tissue development, expansion and regeneration. *Nat Med*. 2013;19(10):1338-44.
20. Wang QA, Song A, Chen W, Schwalie PC, Zhang F, Vishvanath L, et al. Reversible De-differentiation of Mature White Adipocytes into Preadipocyte-like Precursors during Lactation. *Cell Metabolism*. 2018;28(2):282-8.e3.
- 405 21. Childs BG, Baker DJ, Wijshake T, Conover CA, Campisi J, and Van Deursen JM. Senescent intimal foam cells are deleterious at all stages of atherosclerosis. *Science*. 2016;354(6311):472-7.
22. Baker DJ, Childs BG, Durik M, Wijers ME, Sieben CJ, Zhong J, et al. Naturally occurring p16 Ink4a-positive cells shorten healthy lifespan. *Nature*. 2016;530(7589):184.
- 410 23. Ye R, Wang QA, Tao C, Vishvanath L, Shao M, McDonald JG, et al. Impact of tamoxifen on adipocyte lineage tracing: Inducer of adipogenesis and prolonged nuclear translocation of Cre recombinase. *Mol Metab*. 2015;4(11):771-8.
24. Harms M, and Seale P. Brown and beige fat: development, function and therapeutic potential. *Nature medicine*. 2013;19(10):1252.

- 415 25. Chouchani ET, Kazak L, Jedrychowski MP, Lu GZ, Erickson BK, Szpyt J, et al. Mitochondrial ROS regulate thermogenic energy expenditure and sulfenylation of UCP1. *Nature*. 2016;532(7597):112-6.
26. Mills EL, Pierce KA, Jedrychowski MP, Garrity R, Winther S, Vidoni S, et al. Accumulation of succinate controls activation of adipose tissue thermogenesis. *Nature*.  
420 2018;560(7716):102-6.
27. Crewe C, Joffin N, Rutkowski JM, Kim M, Zhang F, Towler DA, et al. An Endothelial-to-Adipocyte Extracellular Vesicle Axis Governed by Metabolic State. *Cell*.  
2018;175(3):695-708 e13.
28. Kazak L, Chouchani ET, Jedrychowski MP, Erickson BK, Shinoda K, Cohen P, et al. A  
425 creatine-driven substrate cycle enhances energy expenditure and thermogenesis in beige fat. *Cell*. 2015;163(3):643-55.
29. Tontonoz P, Hu E, and Spiegelman BM. Stimulation of adipogenesis in fibroblasts by PPAR gamma 2, a lipid-activated transcription factor. *Cell*. 1994;79(7):1147-56.
30. Hu E, Tontonoz P, and Spiegelman BM. Transdifferentiation of myoblasts by the  
430 adipogenic transcription factors PPAR gamma and C/EBP alpha. *Proceedings of the national academy of sciences*. 1995;92(21):9856-60.
31. Wang QA, Tao C, Jiang L, Shao M, Ye R, Zhu Y, et al. Distinct regulatory mechanisms governing embryonic versus adult adipocyte maturation. *Nature cell biology*.  
2015;17(9):1099.
- 435 32. Inagaki T, Sakai J, and Kajimura S. Transcriptional and epigenetic control of brown and beige adipose cell fate and function. *Nat Rev Mol Cell Biol*. 2016;17(8):480-95.

33. Lin J, Wu H, Tarr PT, Zhang C-Y, Wu Z, Boss O, et al. Transcriptional co-activator PGC-1 $\alpha$  drives the formation of slow-twitch muscle fibres. *Nature*. 2002;418(6899):797.
34. Lin J, Tarr PT, Yang R, Rhee J, Puigserver P, Newgard CB, et al. PGC-1 $\beta$  in the regulation of hepatic glucose and energy metabolism. *Journal of Biological Chemistry*. 2003;278(33):30843-8.
35. Rajakumari S, Wu J, Ishibashi J, Lim H-W, Giang A-H, Won K-J, et al. EBF2 determines and maintains brown adipocyte identity. *Cell metabolism*. 2013;17(4):562-74.
36. He C, Hu X, Weston TA, Jung RS, Heizer P, Tu Y, et al. NanoSIMS imaging reveals unexpected heterogeneity in nutrient uptake by brown adipocytes. *Biochem Biophys Res Commun*. 2018;504(4):899-902.
37. Morrison SF, Madden CJ, and Tupone D. Central neural regulation of brown adipose tissue thermogenesis and energy expenditure. *Cell Metab*. 2014;19(5):741-56.
38. Jiang H, Ding X, Cao Y, Wang H, and Zeng W. Dense Intra-adipose Sympathetic Arborizations Are Essential for Cold-Induced Beiging of Mouse White Adipose Tissue. *Cell Metab*. 2017;26(4):686-92 e3.
39. Chi J, Wu Z, Choi CHJ, Nguyen L, Teegene S, Ackerman SE, et al. Three-Dimensional Adipose Tissue Imaging Reveals Regional Variation in Beige Fat Biogenesis and PRDM16-Dependent Sympathetic Neurite Density. *Cell Metab*. 2018;27(1):226-36 e3.
40. Jung RT, Shetty PS, James WP, Barrand MA, and Callingham BA. Reduced thermogenesis in obesity. *Nature*. 1979;279(5711):322-3.
41. Yoneshiro T, Aita S, Matsushita M, Okamatsu-Ogura Y, Kameya T, Kawai Y, et al. Age-Related Decrease in Cold-Activated Brown Adipose Tissue and Accumulation of Body Fat in Healthy Humans. *Obesity*. 2011;19(9):1755-60.

- 460 42. Tajima K, Ikeda K, Chang H-Y, Chang C-H, Yoneshiro T, Oguri Y, et al. Mitochondrial lipoylation integrates age-associated decline in brown fat thermogenesis. *Nature Metabolism*. 2019;1(9):886-98.
43. Iwabu M, Yamauchi T, Okada-Iwabu M, Sato K, Nakagawa T, Funata M, et al. Adiponectin and AdipoR1 regulate PGC-1 $\alpha$  and mitochondria by Ca<sup>2+</sup> and AMPK/SIRT1. *Nature*. 2010;464(7293):1313.
- 465 44. Kusminski CM, Holland WL, Sun K, Park J, Spurgin SB, Lin Y, et al. MitoNEET-driven alterations in adipocyte mitochondrial activity reveal a crucial adaptive process that preserves insulin sensitivity in obesity. *Nat Med*. 2012;18(10):1539-49.
45. Qiao L, Kinney B, Yoo HS, Lee B, Schaack J, and Shao J. Adiponectin increases skeletal muscle mitochondrial biogenesis by suppressing mitogen-activated protein kinase phosphatase-1. *Diabetes*. 2012;61(6):1463-70.
- 470 46. Bukowiecki LJ, Geloan A, and Collet AJ. Proliferation and differentiation of brown adipocytes from interstitial cells during cold acclimation. *The American journal of physiology*. 1986;250(6 Pt 1):C880-7.
- 475 47. Lee YH, Petkova AP, Konkar AA, and Granneman JG. Cellular origins of cold-induced brown adipocytes in adult mice. *FASEB journal : official publication of the Federation of American Societies for Experimental Biology*. 2015;29(1):286-99.

## Figure and figure legends

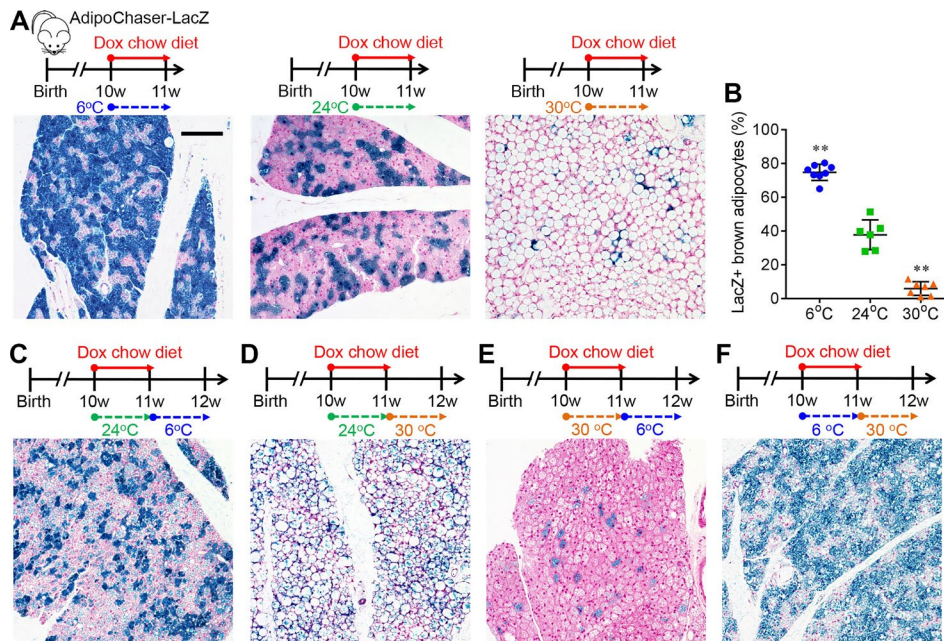


**Figure 1. Two subpopulations of “classical” brown adipocyte undergo dynamic inter-conversions in vivo.** (A) Representative X-gal staining of BAT from AdipoChaser-LacZ mice exposed to different environmental temperatures, while fed with dox-containing chow diet. (B) Quantification of the percentage of LacZ-positive brown adipocytes in the total brown adipocytes.  $n = 8$  mice (6°C); 6 mice (24°C); 7 mice (30°C). (C–F) Representative X-gal staining of BAT from AdipoChaser-LacZ mice kept at indicated temperatures while fed with dox-containing chow diet, followed by regular chow diet feeding at indicated temperatures. Scale bar for A and C–F: 100  $\mu\text{m}$ . All data represent mean  $\pm$  s.d. of biologically independent samples,  $**P < 0.01$ . Statistical significance was assessed using a one-way ANOVA followed by Tukey’s multiple comparisons test. All images are representative of three independent experiments.

485

490

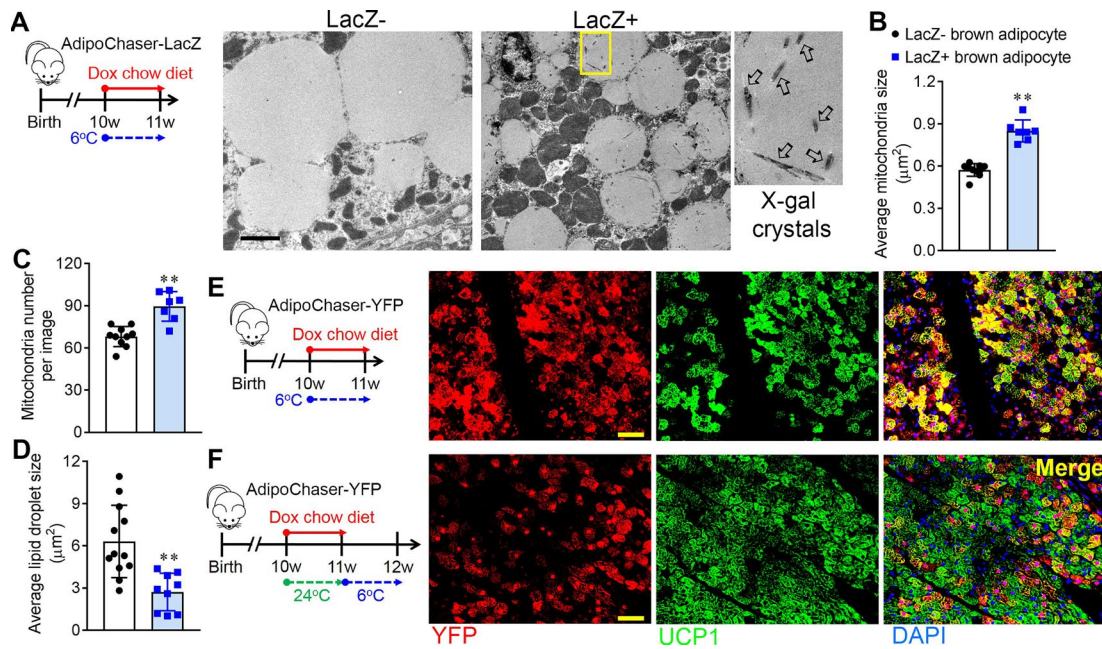
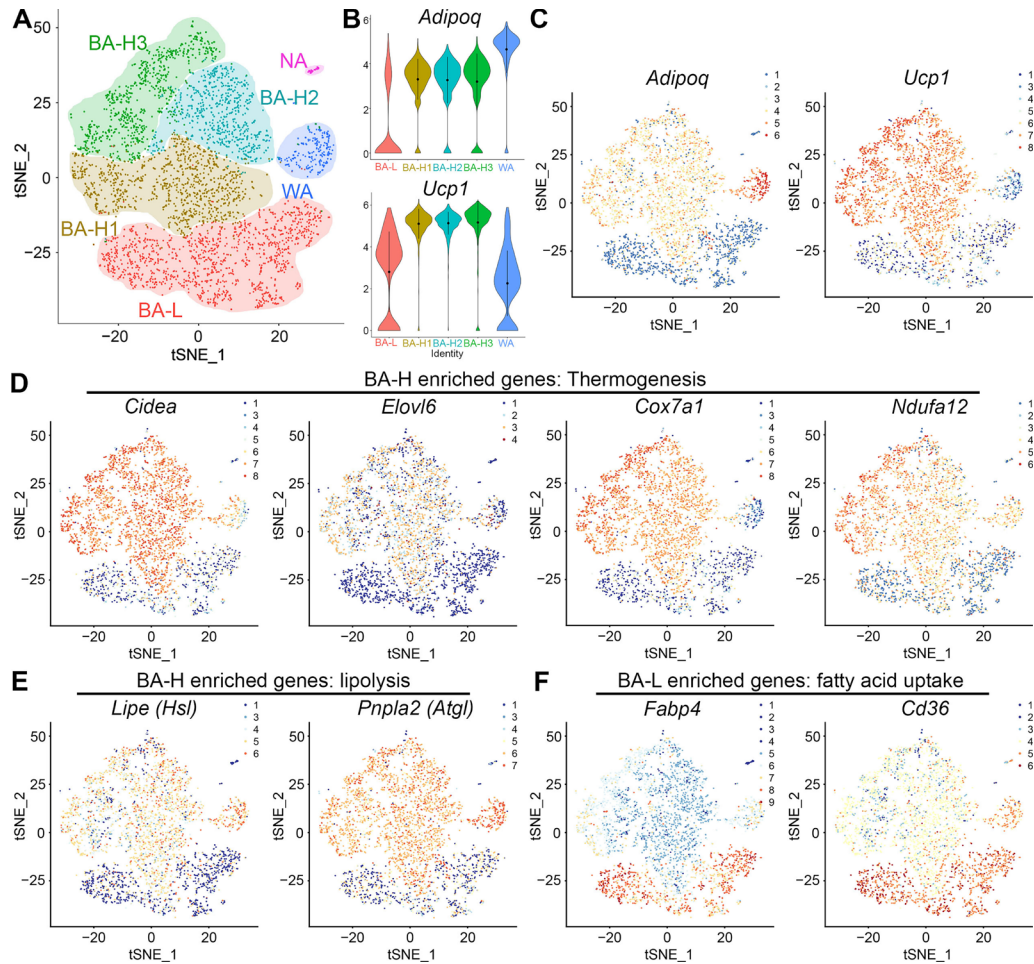


**Figure 2. The two brown adipocyte subpopulations have distinct morphology and *Ucp1* expression.** (A) Electron micrographs of BAT from mice kept at 6°C. Arrows: LacZ crystals. Scale bar: 2 μm. (B–D) Quantification of the mitochondria size, number, and lipid droplet size.  $n = 10$  LacZ+ cells for B and C,  $n = 12$  LacZ+ cells for D;  $n = 7$  LacZ- cells for B–D. (E, F) YFP (red), UCP1 (green) and DAPI (blue) immunofluorescence staining of BAT from AdipoChaser-YFP mice treated with dox-containing chow diet as indicated. Cells with yellow color are double positive with YFP and UCP1. Scale bar: 50 μm. All data represent mean ± s.d. of biologically independent samples, \*\* $P < 0.01$ . Statistical significance was assessed using a two-tailed Student's t-test (B–D). All images are representative of three independent experiments.

495

500



505 **Figure 3. Single-cell RNA sequencing confirms the existence of two distinct brown adipocyte subpopulations.** (A) t-distributed stochastic neighbor embedding (tSNE) plot of 3602 primary brown adipocytes isolated from 10-week-old wide type male mice. Clustering was generated using k-means = 4. This data is from a single experiment. (B–F) Transcript counts represent Log<sub>2</sub> of gene expression. Each dot corresponds to one single cell, colored according to cell cluster. (B) 510 Violin plots showing the distribution of normalized expression values of Adiponectin (*Adipoq*) and *Ucp1* across cells that belong to the five adipocyte clusters. (C–F) Distribution of the expression of *Adipoq* and *Ucp1* (C), *Cidea*, *Elovl6*, *Cox7a1* and *Ndufa12* (D), *Lipe* (*Hsl*) and *Pnpla2* (*Atgl*) (E), and *Fabp4* and *Cd36* (F) within tSNE plot.

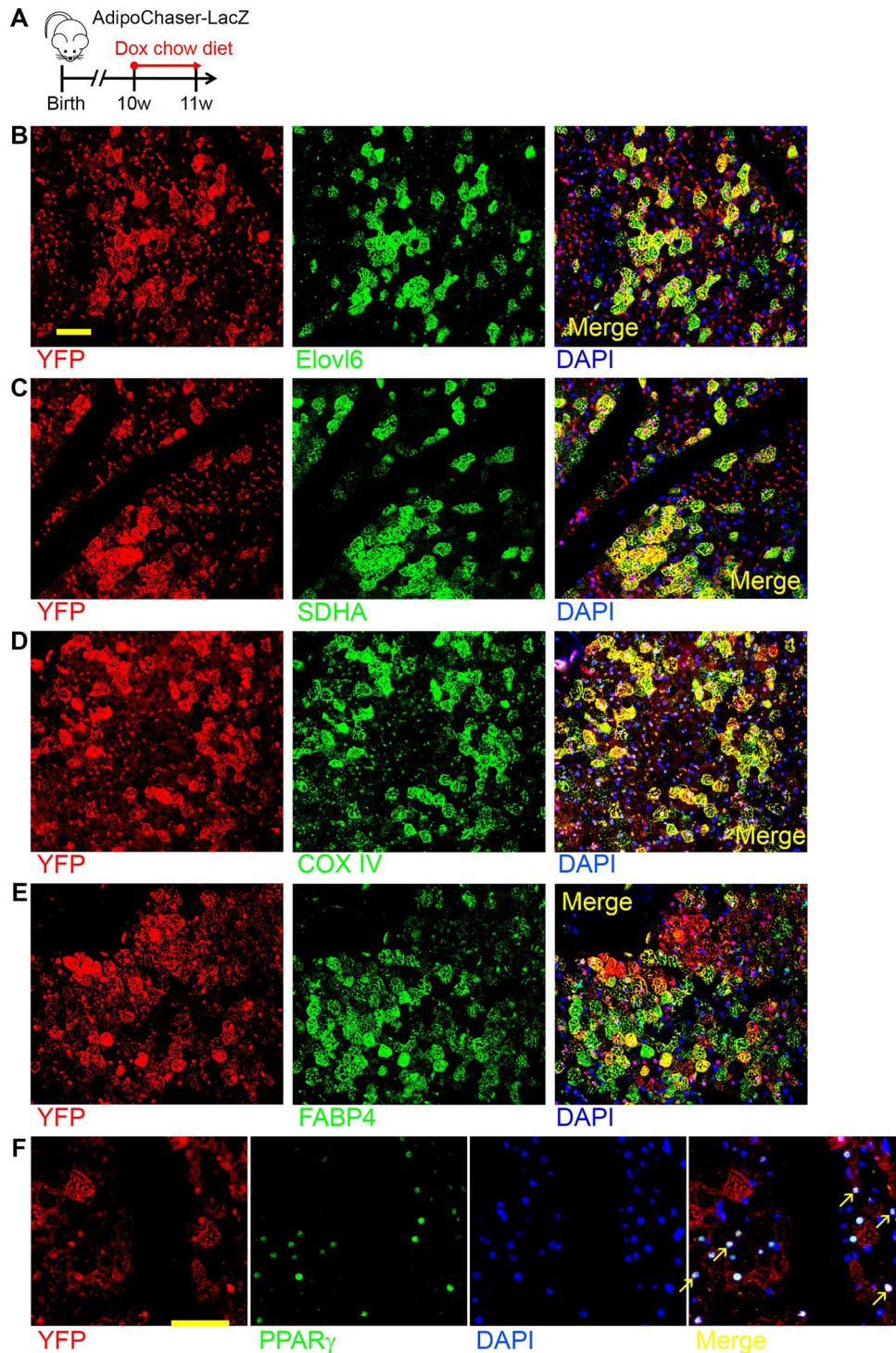


**Figure 4. Immunofluorescence co-staining of differentially expressed genes identified through Single-cell RNA sequencing.** (A) AdipoChaser-YFP male mice were kept on normal chow until 10 weeks of age. Mice were then treated with dox-containing chow diet for one week. (B–F) YFP (red) and Elov16 (green) (B), SDHA (green) (C), COXIV (green) (D), FABP4 (green) (E), and PPAR $\gamma$  (green) (F) immunofluorescence staining of BAT from AdipoChaser-YFP mice treated with dox-containing chow diet as indicated. Cells with yellow color are merged from red and green. Scale bar: 50  $\mu$ m. Images are representative of two independent experiments.

515

520

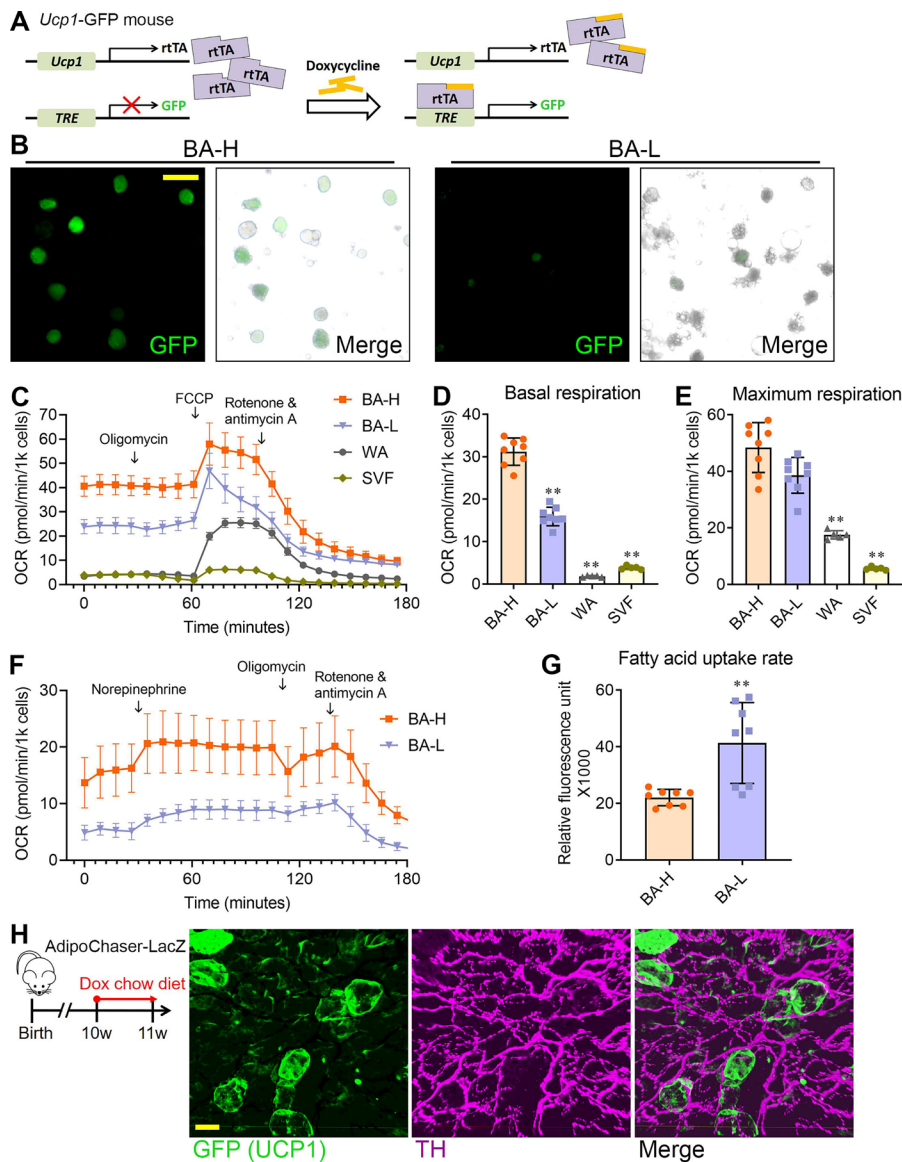
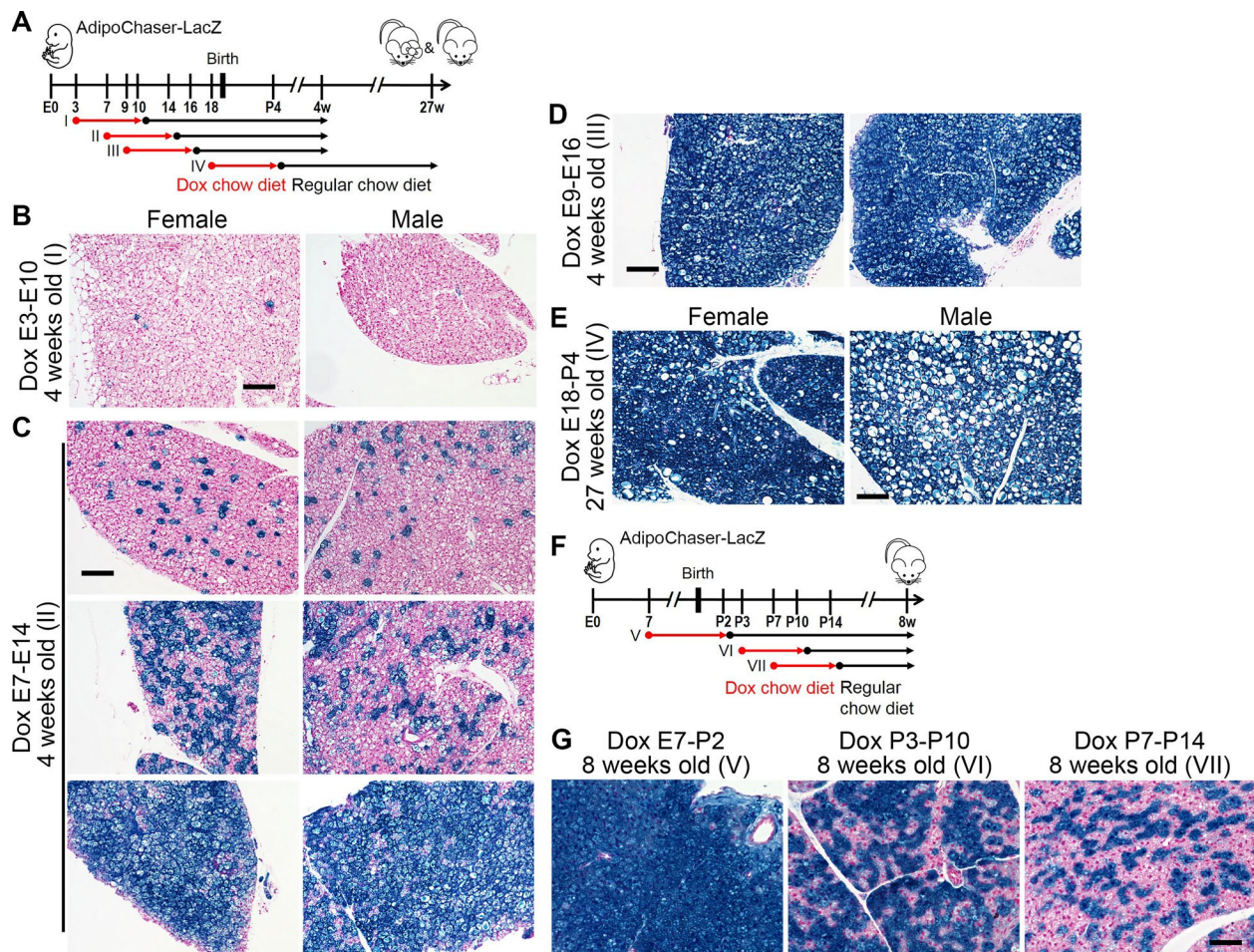


**Figure 5. The brown adipocyte subpopulations have distinct metabolic profiles.** (A) *Ucp1*-GFP mice, the inducible real-time labeling system of *Ucp1* promoter activity, derived from interbreeding two transgenic strains: *Ucp1*-rtTA and TRE-GFP, which allows inducible real-time labeling of the *Ucp1* promoter activity. (B) Fluorescent images of isolated BA-H and BA-L subpopulations from the BAT of *Ucp1*-GFP mice. Scale bar: 50  $\mu$ m. These images are representative of four independent experiments. (C–E) Oxygen consumption rate (OCR) in freshly isolated primary cells, treated with the different compounds. Primary brown adipocytes (BA-H and BA-L) were from male WT mice housed in 6°C for 7 days.

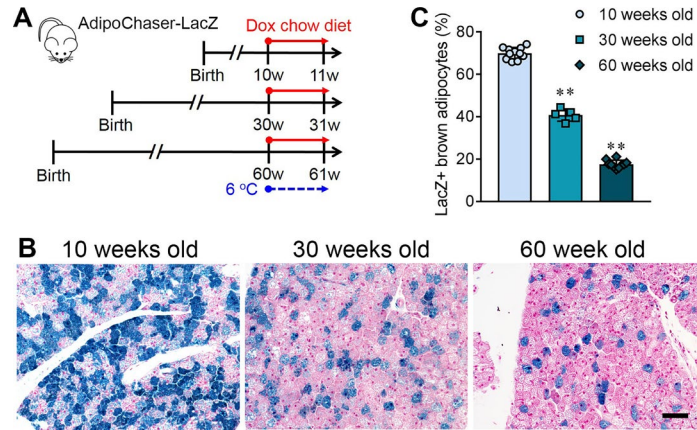
555 As controls, primary white adipocytes and SVF from BAT were from male WT mice housed at room temperature. (C) Plot of OCR to time measured by Seahorse. (D, E) calculated basal and maximum respiration levels of different cell types.  $n = 8$  mice (BA-H and BA-L); 3 mice (WA and SVF). (F) Plot of OCR to time measured by Seahorse in primary brown adipocytes (BA-H and BA-L), treated with the different compounds. These cells were freshly isolated from male AdipoChaser-mT/mG mice housed in 6°C for 7 days through EasySep™ Magnet. (G) Fatty acid uptake rate in the two brown adipocyte subpopulations.  $n = 8$  mice (BA-H and BA-L). For each group, cells from all mice were pooled together, and data represent mean  $\pm$  s.d. of experimental replicates, normalized to cell numbers. \*\* $P < 0.01$ . Statistical significance was assessed using a one-way ANOVA followed by Tukey's multiple comparisons test (D, E), or a two-tailed Student's t-test (G). (H) 10 weeks old *Ucp1*-GFP mice were treated with dox-containing diet for 4 days before tissue harvest. PACT-cleared BAT from *Ucp1*-GFP mice and immunolabeled with GFP (green) and sympathetic neuron marker tyrosine hydroxylase (TH) (purple) antibody. Scale bar: 30  $\mu$ m. These images are representative of three independent experiments.

560

565



570 **Figure 6. Brown adipocyte were born as adiponectin high expressors, and the heterogeneity**  
**establishes postnatally.** (A) Female mice carrying only *Adn-rtTA* and *Rosa26-loxP-stop-loxP-*  
575 *LacZ* were bred with *AdipoChaser-LacZ* male mice. When these female mice were pregnant, they  
were exposed to dox-containing chow diet during E3–E10, E7–E14, E9–E16, or E18–P4, and kept  
on regular chow diet thereafter. Offspring of these female mice were genotyped, and  
*AdipoChaser-LacZ* mice of both genders were used for LacZ staining when they were 4 weeks or  
27 weeks old. (B–D) Representative X-gal staining of BAT from 4-week-old *AdipoChaser-LacZ*  
580 mice that were on dox diet for the indicated number of days during development. (E)  
Representative X-gal staining of BAT from 27-week-old *AdipoChaser-LacZ* mice that were on  
dox diet during E18–P4. Scale bar for B–E: 100  $\mu$ m. (F) Female mice carrying only *Adn-rtTA*  
and *Rosa26-loxP-stop-loxP-LacZ* were bred with *AdipoChaser-LacZ* male mice. When these  
585 female mice were pregnant, they were exposed to dox-containing chow diet during E7–P2, P3–  
P10, or P7–P14, and kept on regular chow diet thereafter. Offspring of these female mice  
were genotyped, and male *AdipoChaser-LacZ* mice were used for LacZ staining when they were 8  
weeks old. (G) Representative X-gal staining of BAT from these *AdipoChaser-LacZ* mice that  
were on dox diet for the indicated number of days during development. Scale bar: 50  $\mu$ m. All  
images are representative of three independent experiments.



590

**Figure 7. The recruitment of BA-H during cold exposure is declined with age.** (A) AdipoChaser-LacZ male mice were kept on normal chow until 30 or 60 weeks of age. Mice were then exposed to 6°C for 7 days while treated with dox-containing chow diet. (B) Representative X-gal staining of BAT from mice of different age exposed to 6°C. Scale bar: 50 μm. (C) Quantification of the percentage of LacZ-positive brown adipocytes in the total brown adipocytes. *n* = 11 mice (10 weeks old); 5 mice (30 weeks old); 10 mice (60 weeks old). \*\**P* < 0.01. Statistical significance was assessed using a one-way ANOVA followed by Tukey's multiple comparisons test. All images are representative of three independent experiments.

595